Carbon Nanotube-Induced Loss of Multicellular Chirality on Micropatterned Substrate Is Mediated by Oxidative Stress

Ajay V. Singh,[†] Krunal K. Mehta,[‡] Kathryn Worley,[†] Jonathan S. Dordick,[‡] Ravi S. Kane,[‡] and Leo Q. Wan[†,*]

[†]Department of Biomedical Engineering, Center for Biotechnology & Interdisciplinary Studies, Rensselaer Polytechnic Institute, Troy, New York 12180, United States and [‡]Department of Chemical and Biological Engineering, Center for Biotechnology & Interdisciplinary Studies, and Rensselaer Nanotechnology Center, Rensselaer Polytechnic Institute, Troy, New York 12180, United States

ABSTRACT Carbon nanotubes (CNTs) are receiving much attention in medicine, electronics, consumer products, and next-generation nanocomposites because of their unique nanoscale properties. However, little is known about the toxicity and oxidative stress related anomalies of CNTs on complex multicellular behavior. This includes cell chirality, a newly discovered cellular property important for embryonic morphogenesis and demonstrated by directional migration and biased alignment on micropatterned surfaces. In this study, we report the influence of single-walled carbon nanotubes (SWCNTs) on multicellular chirality. The incubation of human umbilical vein endothelial cells (hUVECs) and mouse myoblasts (C2C12) with CNTs at different doses and time points stimulates reactive oxygen species (ROS) production and intra- and extracellular oxidative stress (OS). The OS-mediated noxious microenvironment influences vital subcellular organelles (*e.g.*, mitochondria and centrosomes), cytoskeletal elements (microtubules), and vinculin rich focal adhesions. The disorientated nuclear−centrosome (NC) axis and centriole disintegration lead to a decreased migration rate and loss of directional alignment on micropatterned surfaces. These findings suggest that CNT-mediated OS leads to loss of multicellular chirality. Furthermore, the *in vitro* microscale system presented here to measure cell chirality can be extended as a prototype for testing toxicity of other nanomaterials.

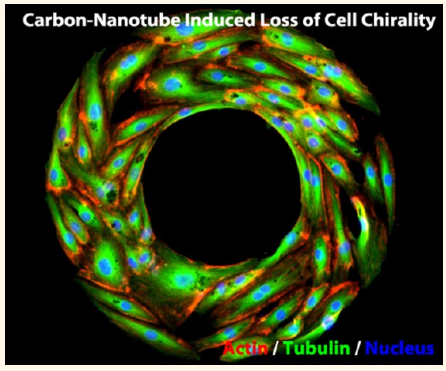

KEYWORDS: single-walled carbon nanotubes (SWCNTs) · cell chirality · left−right asymmetry · micropatterning · oxidative stress

In the past 20 years, a variety of nanomaterials have revolutionized biomedicine. They have been engineered and customized into nanoscale constructs with payloads for imaging and chemotherapeutics.[1,2] Carbon-based nanomaterials, such as single-walled carbon nanotubes or SWCNTs, have drawn much attention due to their superior mechanical and chemical properties.[3,4] SWCNTs have demonstrated enormous potential applications in tissue engineering (due to their high stiffness and one-dimensional geometry),[4−6] biosensing (due to functionalization opportunities and hydrophobicity that allows the binding with proteins, peptides and antibodies),[7,8] intracellular probing (due to their nanoscale diameter)[9] and photothermal imaging and therapy in cancer (due to optoelectronic properties).[4,6,7,10] Furthermore, the unique morphology, crystalline structure, and high surface area of CNTs enhance their interactions with the cell membrane and give snaking access to enter into the cell.[11] Their one-dimensional (1D) characteristics, wall rigidity, and flexibility have been attributed to serious cell injury and asbestos-like carcinogenic toxicity.[12] While no human pathology has been reported thus far due to CNT exposure, single and multiwall CNTs have been shown to elicit adverse inflammatory cascades, such as frustrated phagocytosis, genotoxic responses, and oxidative stress.[13−15] Therefore, it is necessary to understand CNTs toxicity and its implications due to their widespread human exposure in occupational and consumer settings.[16]

* Address correspondence to wanq@rpi.edu.

Received for review October 8, 2013 and accepted February 23, 2014.

Published online February 24, 2014
10.1021/nn405253d

Oxidative stress is one of the most common hazardous manifestations of CNTs.[17] In particular, cells lining the epithelium of skin and endothelium of blood vessels, which come in close contact with nanomaterials when adsorbed or inhaled *in vivo*, are most affected.[18,19] The use of as much as 30% of transition-metal catalysts, predominantly iron, nickel and cobalt in CNT manufacturing processes, are sources of reactive oxygen species (ROS).[17] Postmanufacturing processing for research and clinical application removes the majority of metal impurities; however, partial encasement within CNTs makes complete removal impossible.[19] Therefore, health hazards associated with CNTs are not only due to the CNT itself, but also potential metallic components. The safety of these materials needs to be evaluated in consumer, environmental and occupational settings.[13]

To date, the evaluation of nanotoxicity has been limited to biochemical quantification of glutathione (GSH) depletion, protein oxidation, lipid peroxidation, and total antioxidant capacity.[19] Previous reports investigated the mechanistic toxicity of raw SWCNTs at a molecular level and found that they interfered signal transduction and key molecular events involved in mesothelioma development.[20,21] In addition, *in vitro* models also reported that CNTs mediated the induction of inflammatory cytokines and cellular responses under static and dynamic culture conditions.[22−25] None of the reports, however, have systematically evaluated the impact of CNT-mediated oxidative stress (OS) on complex cell behavior at a multicellular level, including collective behavior in alignment and migration that is important for multicellular morphogenesis during tissue development. These issues are of paramount importance in light of the transition of CNTs from research to clinical practice.[26] Recently, we have demonstrated that mammalian cells exhibit phenotype specific left−right (LR) asymmetry (also known as handedness or chirality) when micropatterned on fibronectin coated cell adhesive geometries.[27,28] This micropatterning system gives us the opportunity to study developmental toxicity at a multicellular level, and the potential to use cell chirality as a biomarker to evaluate alterations in cell function due to nanomaterial toxicity. This novel approach could set forth a paradigmatic *in vitro* model for assessing the risk of CNTs and other emerging materials through evaluating collective cell behavior.

In this study, the possible cytotoxicity of SWCNTs is evaluated with endothelial cells and myoblasts on micropatterned cell adhesive surfaces. In particular, we explore the influence of CNT exposure on cell chiral morphogenesis and the role of oxidative stress (OS) and subcellular organelle damage. We find that when incubated with CNTs, both cell types show a dose- and time-dependent loss of chirality due to intra- and extracellular OS induced by CNTs. In-depth analyses reveal disintegrated centrosomes, disorganized microtubulin networks, matured adhesion complexes, and decreased cell migration. These results suggest that nanomaterial toxicity can be tested by evaluating the function of cellular chiral machinery, a potentially important measure for developmental toxicology.

RESULTS

Exposure to SWCNTs Induces Loss of Cell Chirality. Cell chirality is an important cell function associated with embryonic development of LR asymmetry.[29] To study effects of cellular exposure to nanoparticles on chirality, we treated human umbilical vein endothelial cells (hUVECs) and mouse C2C12 myoblasts with SWCNTs on micropatterned surfaces (Figures 1 and S1, Supporting Information).[30] Without CNTs, both cell types formed chiral alignment on micropatterned rings, as demonstrated previously.[27] phase contrast images of hUVECs on fibronectin-coated ring-shaped micropatterns were taken (Figure 1A), and cell alignment was determined with a custom-written MatLab program and shown with orange lines (Figure 1B). On the basis

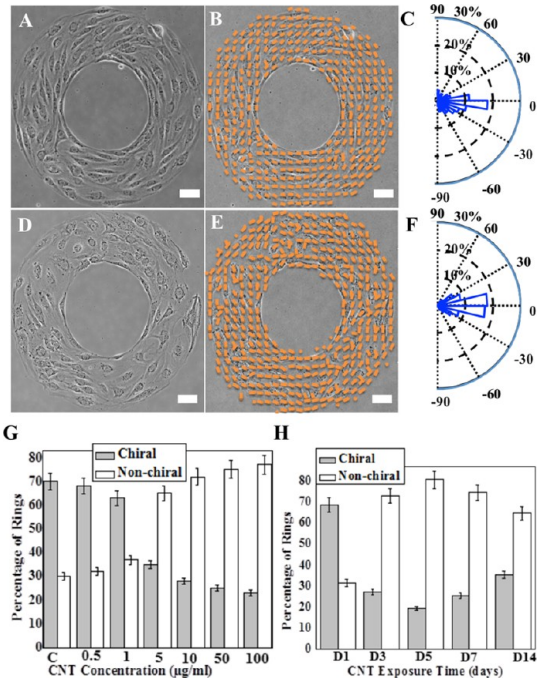

Figure 1. Endothelial cells lose chirality in presence of carbon nanotubes (CNTs). (A) A phase contrast image of asymmetric cell alignment of endothelial cells on ring patterns without the CNTs. (B) Local cell alignment of (A) determined with an automatic MatLab program and indicated with short orange lines. (C) The circular histogram of biased angles (based on the deviation of short orange lines in (B) from the circumferential direction) shows a CW bias in endothelial cells. (D−F) Endothelial cells incubated with CNTs show no preference in left−right asymmetry on appositional boundaries (D) as indicated in cell alignment (E) as well as measured biased angles (F). (G) The percentage of chiral rings decreases with CNT concentration after 3-day exposure. (H) Time-dependent chirality loss of endothelial cells when exposed to 10 μg/mL of CNT. Scale bars: 50 μm.

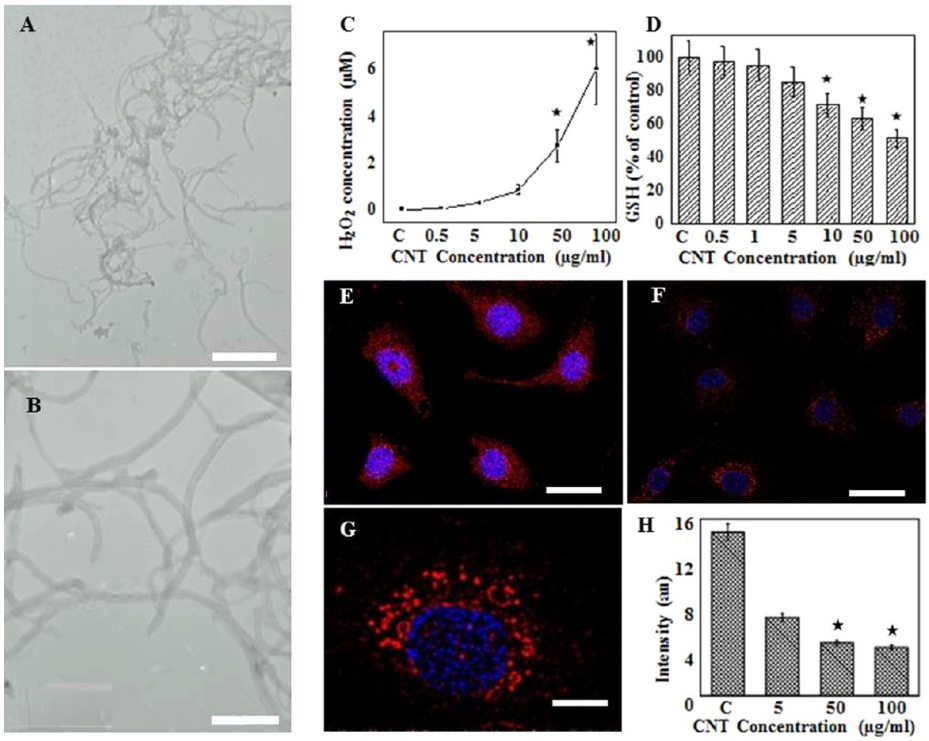

Figure 2. CNTs induce mitochondrial oxidative stress. (A,B) Transmission electron microscope (TEM) images of carbon nanotubes. (C) Hydrogen peroxide production (an extracellular oxidative stress indicator) as a function of CNT concentration. (D) Glutathione (an intracellular antioxidant preventing reactive oxidative stress-induced cellular damages) decreased with CNT concentration. (E) Mitochondria staining in hUVECs control, as well as (F) in the cells treated with 10 μg/mL of CNTs for 24 h. (G) A magnified image showing concentrated mitochondrial staining in vicinity of the perinuclear region. (H) Quantified integrated fluorescence density of Mitotracker stain in the cells (n = 40−50) of control and test groups. Bars represent standard error. Scale bars in (A) 50 nm; (B) 20 nm, (E,F) 40 μm; (G) 10 μm.

of their deviation from the circumferential direction, biased angles between 90° and −90° were assigned (Figure S2C, Supporting Information), and a positive value represents a counter clockwise (CCW) alignment, while a negative value represents a clockwise (CW) alignment. The circular histogram plot (Figure 1C) reveals that biased angles had a preference for negative values, corresponding to a CW bias of hUVECs control (*i.e.*, without CNTs exposure). In contrast, CNT-treated hUVECs showed no preference and exhibited an unbiased or nonchiral behavior (Figure 1D−F). On the other hand, C2C12 cells exhibited a CCW bias in the control, but no bias in the CNT-treated sample (Figure S2A,B, Supporting Information).

CNTs Affect Multicellular Chirality in a Dose- and Time-Dependent Manner. We then evaluated the effects of CNT concentration and exposure time on multicellular chirality of both hUVECs (Figure 1G,H, Table S1, Supporting Information) and C2C12 cells (Figure S2, Table S2, Supporting Information) on ring-shaped micropatterns. The gradual loss of chirality with hUVECs was found to depend on CNT concentration. The cells were treated with CNTs for 3 days at concentrations ranging from 0.5 to 100 μg/mL. The hUVECs exhibited a CW dominant alignment (~70% CW) at a CNT concentration of 1 μg/mL or below, although the percentage of chiral rings decreased with CNT concentration. When the concentration exceeded 5 μg/mL, far below the widely reported toxic concentration of 100 μg/mL, the cells began to lose chirality.[31] Even at 5 μg/mL, more than 65% patterned rings did not show a CW preference, when compared to only 30% for the control group. A similar trend was observed for C2C12 cells, and CNTs at 10 μg/mL or above induced nonchiral behavior on patterned surfaces.

The CNT exposure time with hUVECs (Figure 1H) and C2C12 cells (Figure S2D,E and Tables S3 and S4, Supporting Information) also affected measured cell chirality. An initial 24 h exposure of CNTs did not affect hUVECs intrinsic CW alignment, but incubation of cells with nanotubes beyond 72 h (3, 5, 7, and 14 days *in vitro*: DIV) significantly discouraged these endothelial cells to align in a biased fashion (Figure 1H) with less than 25% of endothelial cell patterns demonstrating chirality. The C2C12 cell line exhibited greater tolerance toward CNT exposure, and the cells lost chiral behavior over a longer exposure time, typically 5 days.

CNTs Induce Oxidative Stresses. To explore the underlying mechanisms of CNT-induced loss of cell chirality, we first examined whether cell metabolism was significantly altered by CNTs, using the MTT assay. hUVECs were cultured with CNTs at different concentrations

(0.5−100 μg/mL) for 24 h. A significant difference in cell metabolism was only found at a high dose (50−100 μg/mL) (Figure S3B, Supporting Information; $p < 0.0001$ for control *vs* 100 μg/mL). However, the threshold concentration of CNTs switching multicellular behavior from chiral to nonchiral is as low as 5 μg/mL. This indicates that the loss of cell chirality is not likely caused by any significant changes in cell viability or metabolism, and that cell chirality may be a more sensitive measure for toxicity than other assays that detect cell viability, proliferation, and/or cellular metabolism.

The physical and mechanical properties of CNTs, such as rigidity and large aspect ratios (length/diameter), have been attributed to cell injury. The dimensions of CNTs were quantified in transmission electron microscope (TEM) images (Figure 2A,B), given an average diameter of 5.0 ± 0.5 nm and a length of 265 ± 110 nm. The CNTs formed entangled shapes, which were reported to cause less cell injury and inflammation.[12]

We then evaluated possible effects of oxidative stresses induced by CNTs. Extracellular oxidative stress was measured with Amplex Red hydrogen peroxide (H_2O_2) detection kit, and H_2O_2 was found to increase significantly with the CNT concentration (Figure 2C). The H_2O_2 most likely arises as a result of traces of metallic precursors present in CNTs as impurities when prepared *in situ*.[1] Intracellular oxidative stress was assessed *via* glutathione quantification (Figure 2D) and mitochondrial staining (Figure 2E−H). Intracellular glutathione in its reduced form (GSH) decreased with the CNT concentration, indicating an increase of oxidative stress with the CNT treatment. The hUVEC control (Figure 2E) had a stronger staining with an even distribution throughout the cells, while mitochondria are less and more concentrated around the perinuclear region in the CNT-treated cells (Figure 2F,G). These findings were further confirmed with the quantification of integrated fluorescence intensity of mitochondria (Figure 2H) and a 3D surface plot of fluorescence intensity (Figure S3A, Supporting Information). Altogether, our data indicate the likelihood of CNT-induced cellular oxidative stress, and possibly mitochondrial damage.[32]

Intra- and Extracellular ROS Scavengers Recover Cell Chirality. We proceeded to investigate whether the loss of chirality is directly linked with intra- and extracellular oxidative stress. To answer this question, we subjected CNT-treated hUVECs with ROS scavengers or inhibitors including catalase (an enzyme catalyzing the decomposition of H_2O_2 into oxygen and water), mannitol (a superoxide anion and hydroxyl radical quencher), and diphenyleneiodonium chloride (DPI; an inhibitor of NO synthase and NADPH oxidases) for 3 days (Figure 3, Table 1). In all cases, the cells exhibited a dominantly clockwise chirality, with a 60% of clockwise rings, similar to the hUVECs control (without CNTs or any drugs), while the CNT-treated group had over 60% rings showing a predominantly nonchiral behavior. To further confirm the role of H_2O_2 generated by CNTs in loss of cell chirality (Table 2), we directly treated the hUVECs with a similar level of H_2O_2 (10 μM), and the number of nonchiral rings was found to increase significantly, as observed with the CNT-treated group.

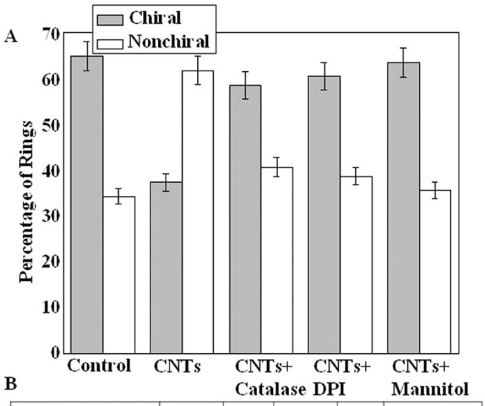

B

Experimental descriptions	No of Rings	CW	CCW	NC	P-value
Control	168	110	5	53	p < 0.0001
CNTs	162	52	9	101	p < 0.0001
CNTs+Catalase	155	91	3	61	p < 0.001
CNTs+DPI	135	82	2	51	p < 0.001
CNTs+Mannitol	149	95	10	44	p < 0.0001

Figure 3. Free radical scavenger treatment reverts endothelial chirality. (A) Bar graph demonstrates that peroxide scavenger catalase (50 U/mL) ROS quencher Mannitol (20 mM) and intracellular OS inhibitor DPI (1 μM) induce cell chirality and preserve clockwise alignment of cells on micropatterns. (B) Table shows quantified clockwise and nonchiral cells (data: mean ± standard error; CW, clockwise; CCW, counterclockwise).

TABLE 1. Role of Carbon Nanotubes (CNTs) and Extracellular Oxidative Stress in the Loss of Endothelial Cell Chirality (CNTs: 10 μg/mL, Catalase: 50 U/mL, and H_2O_2: 10 μM)

experimental description	number of rings	CW	CCW	NC	*p*-value
control	85	**56**	0	29	<0.001
CNTs	81	25	5	**51**	<0.0001
CNTs + catalase	74	39	1	34	>0.05
H_2O_2	78	29	0	**49**	<0.01
H_2O_2 + catalase	52	28	1	23	>0.05
catalase	54	**33**	1	20	<0.05

TABLE 2. Role of Carbon Nanotube-Induced Intracellular Oxidative Stress in the Loss of Endothelial Cell Chirality (CNTs: 10 μg/mL, DPI: 1 μM, and Mannitol: 20 mM)

experimental description	number of rings	CW	CCW	NC	*p*-value
control	81	**49**	3	19	<0.0001
CNTs	81	25	5	**51**	<0.0001
DPI	66	29	6	31	>0.05
CNTs + DPI	73	**45**	3	25	<0.001
CNTs + mannitol	77	**51**	7	19	<0.0001

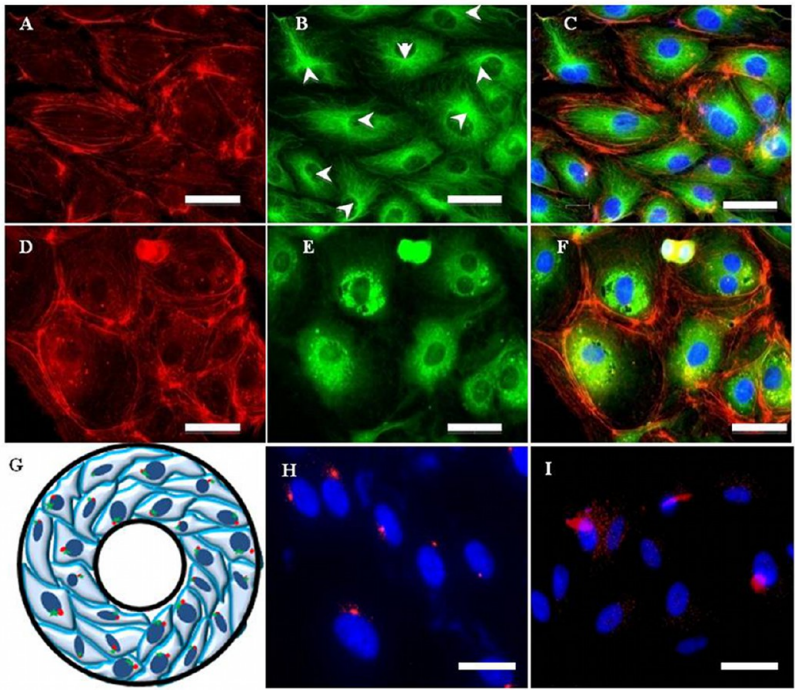

Figure 4. Cytoskeleton staining and nucleus−centrosome (NC) positioning. (A−C) Actin (red), tubulin (green), and nucleus (blue) staining of the hUVEC control, showing positioned centrosome (bright green). (D−F) The same staining of endothelial cells with CNT (10 μg/mL) exposure for 24 h. (G) Schematic drawing demonstrating clockwise biased alignment of endothelial cell and NC axis positioning, which supports directional cell migration (blue: nucleus, red: centrosome). (H,I) Pericentrin-DAPI (red-blue) overlay in multicellular hUVEC micropatterns showing NC axis in the control (H) and CNT-treated endothelial cells (I). Scale Bars: 20 μm.

This H_2O_2-induced loss of cell chirality was recovered by the catalase treatment, while catalase alone did not have a significant effect on cell chirality.

CNTs Decrease Cell Migration. LR asymmetry on patterned surfaces is established by a mechanism involving multicellular directional migration on appositional boundaries. The chiral cell alignment requires proper cell polarization on boundaries as well as cell migration. We then measured the speed of hUVECs migration in the presence and absence of CNTs for 24 h. hUVEC migration speed significantly decreased with CNT treatment (Figure S4A, Supporting Information; $p < 0.05$, control *vs* 100 μg/mL of CNTs). This finding sets forth a new paradigm that relates CNT toxicity and cell stress, which subsequently down-regulate cell motility, one of the important parameters determining multicellular chirality *in vitro*.[27] We also measured the cell morphology by calculating cell area as well as cell aspect ratio (defined as distance maxima between leading and trailing edge divided by maximum width passing through cell nuclear axis). The cell area did not change significantly (Figure S3D, Supporting Information), but the cells did appear more elongated, and seemed to adopt fibroblastoid-shape with the CNT treatment (Figure S3D, Supporting Information, and box-whiskers plot in Figure S4B, Supporting Information). ImageJ quantification revealed that major populations of control endothelial cells have aspect ratios (AR) closer to 2.8, whereas in the CNT-treated cells, AR is 3.2.

CNTs Affect Cell Cytoskeleton, Centrosome−Nucleus Positioning, and Focal Adhesion Assembly. Establishing and maintaining subcellular organelle polarity and their mutual positioning are important for directional cell migration.[33,34] In our previous studies, we have shown that the Golgi apparatus, centrosome, and nucleus positioning as well as the cytoskeleton organization are important for preferred endothelial LR alignment on micropatterned geometric boundaries and play a vital role in chirality.[27,28] As a result, we examined whether CNT induced significant alternations in subcellular organelles and cytoskeleton proteins.

To that end, we first stained actin filaments and microtubules. Actin filament cables in CNT-treated endothelial cells were found to be thicker and conspicuously located at cell periphery compared to the control (control: Figure 4A−C; CNTs-treated group: Figure 4D−F). More interestingly, the control endothelial cells exhibited more stable microtubule expression with radial patterns of microtubule distribution, emanating near the nucleus from a bright and well-organized pericentriolar region as shown in Figure 4B (white arrow), while the endothelial cells incubated with CNTs did not show clearly organized tubular structures (Figure 4E). Microtubule staining appeared to be evenly distributed throughout cytoplasm in control cells, whereas in CNT-treated cells, the staining was concentrated in the central region of the cells.

We speculate that the poor organization of microtubules might be the result of the impaired function of the centrosome, as acentrosomal cells were reported to be devoid of radial arrays of astral microtubules as shown in schematic of Figure 4G.[33,35,36] In the pericentrin staining, noticeably, the CNTs indeed caused destruction of centrosome in hUVECs (Figure 4H,I, control and test sample respectively). The orientation of nucleus−centrosome (NC) axis was very well preserved with all cells maintaining a distinct and integrated centrosome in hUVECs control (without CNTs) on patterned boundaries (Figure 4H: red: centrosome, blue: nucleus). Conversely, a clear destruction of centrosome in CNT-incubated endothelial cells was seen, with diffused signals and scattered pericentrin region (Figure 4I). We also did a time- and dose-dependent study of centrosomal organization and observed that its integrity was gradually lost with higher dose ($\geq 10\ \mu$g/mL) or longer exposure (≥ 3 days) (Figures S5B and S6B, Supporting Information).

Focal adhesion complexes (FACs) or cell-matrix adhesions are macromolecular assemblies that function as the cell "stress-sensor".[37] On micropatterned surfaces, focal adhesion assembly has been shown to be intricately related to the molecular force transmission from the surrounding microenvironment.[38] This prompted us to probe the role of FACs to determine if they play a role in inhibiting cell motion and asymmetric alignment. As shown in Figure 5A−D, we observed differences in number, morphology, expression pattern, and distribution in FACs on test and control samples. Endothelial cells cultured without CNTs demonstrated classical vinculin expression distributed as thin, elongated adhesions at cellular peripheral regions as well as some interior regions (Figure 5A). Conversely, CNT-treated cells were more spread, and much larger and more circular FACs were found to distribute mainly along cell periphery (Figure 5B). Magnified images show thick and intense adhesion spots, few in number and positioned along cell boundary in CNT-treated hUVECs (Figure 5D), while numerous, less intense dots distributed through cytoplasm in the control cells (Figure 5C). The lower panel in Figure 5E, F shows a line scan of enlarged image with significantly higher intensity (*y* axis, gray value) and spread area (*x* axis, pixel distance). The measured numerical parameters associated with vinculin structured adhesion complexes (normalized vinculin area, mean value, average pixel intensity and number) were shown in Table S5 (Supporting Information), indicating significant differences in control *versus* the CNT-treated group. We also observed time- and concentration-dependent changes in FACs number, morphology, expression pattern, and distribution. Significant changes occurred at a CNT concentration of larger than 5 μg/mL or an exposure time of 3 days or more (Figures S5C and S6C, Supporting Information).

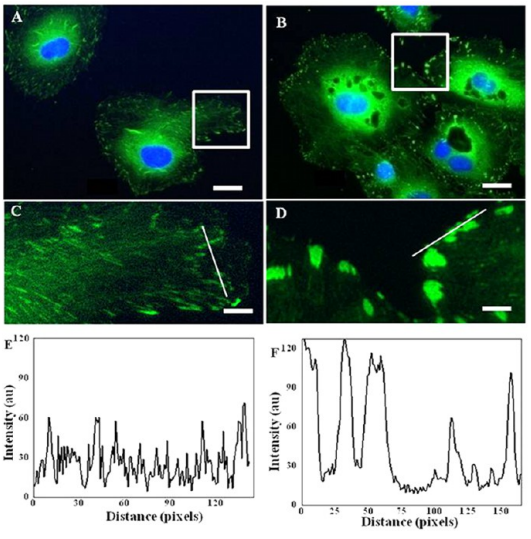

Figure 5. Analyses of focal adhesion morphology. (A,B) Immunostained vinculin-rich focal adhesion complexes (FACs) in hUVECs show differences of FACs in the control (A) and the CNT-treated group (B). (C,D) Magnified images from highlighted regions in (A,B). (E,F) Variations in size, shape, and degree of expression of vinculin in FACs in control (E) and CNT-treated (F) cells. Scale bars: (A,B) 20 μm, (C,D) 5 μm.

DISCUSSION

In recent years, there has been substantial interest in SWCNT-based application as tissue scaffolds for regenerative medicine or intracellular transporters for various therapeutic and diagnostic (theranostic) carrier.[39] However, numerous reports also highlighted safety concerns toward SWCNTs as an alternative of conventional theranostic tools.[40,41] Left−right (LR) asymmetry or chirality has been observed in tissue morphogenesis of numerous living organisms during embryonic development.[42] Recently, we have shown that micropatterned mammalian cells exhibit phenotype-specific biased LR alignment on micropatterned appositional boundaries.[27] Although LR asymmetry is a fundamental process in morphogenesis, it could affect many basic bioengineering phenomena, such as cell migration, wound healing, and tissue growth of unicellular and multicellular system.[30,43] The objective of this study was to exploit this micropatterning-based chiral characteristic of the cell as an *in vitro* approach to investigate potential effects of nanomaterial, specifically SWCNTs on development-related cellular functions.

In this study, we used CNTs at a concentration ranging from 1 to 100 μg/mL. To our knowledge, the exact concentration of CNT exposure at a cellular level in real life has not been reported. However, CNT inhalation in manufacturing industry and intravenous/subcutaneous injection in nanomedicine can potentially lead to the local accumulation of CNTs at high concentrations. As a result, to mimic the industrial exposure of carbon based material to workers, CNTs

are often administered *in vivo* at a high concentration (1−10 mg/mL) and with a dose up to 20 mg/kg of animal body.[19] In *in vitro* experiments, CNTs at up to 1000 μg/mL have been tested for possible toxicity on various types of cells.[18,25] Therefore, the concentrations we used in this study aligned well with published studies, and we believe that they are relevant to the potential CNT exposure in real life.

The cells showed significant differences in their tolerance to CNT toxicity. Incubation of endothelial cells with 5 μg/mL or higher CNTs for more than 24 h led to a loss of preferential CW alignment on micropatterned rings, while the concentration to switch chiral behavior of the C2C12 cell line was 10 μg/mL for 3 days. Such a difference between these two types was in agreement with previous reports.[44] This was expected, as primary cells are typically more sensitive to nanomaterial toxicity; this is also why more emphasis is given toward toxic evaluation of nanomaterials with primary cells, to closely mimic *in vivo* conditions.[13,45]

Oxidative stress was found to be involved in CNT-associated chirality loss of endothelial cells. Indeed, lately there is increasing evidence of CNT cytotoxicity arising due to oxidative stress, and disruption of intracellular metabolic pathways.[46] It has been established that the metal impurities, particularly iron and nickel trapped inside the CNTs, may be partially responsible for OS.[47] These metals produce free hydroxyl and peroxy radicals *via* catalytic degradation of hydrogen peroxide through classic Fenton and Haber−Weiss reactions, which damage cellular DNA, lipids, and proteins.[48] In our experiments, we found that H_2O_2 was produced in culture in CNT-treated groups, and reduced glutathione reductase activity decreased with the increasing CNT concentration. When incubated with H_2O_2 overnight, 65% or more of endothelial cell patterns lost chirality; *i.e.*, more multicellular patterned rings did not show the preferred clockwise bias.[27] Such loss of cell chirality could be recovered with ROS inhibitors such as catalase, mannitol, and DPI (Figure 3). Taken together, the anti-ROS scavenger experiments strengthened the point that oxidative stress is the fundamental cause of lost cell chirality reported here.

The analysis of cellular physiological and molecular machinery responsible for chiral behavior unfolded the OS mediated mechanism. Time-lapse analysis of hUVECs in presence and absence of CNTs environment demonstrated that there is a significant drop in endothelial migration rate when treated with CNTs at high concentrations. Centrosome disintegration was also observed for CNT-treated cells (Figure 4H−I). This suggested a strong connection between the subcellular organelle integrity and its relation with reduced migration, and deprivation of multicellular LR alignment on ring micropatterns. This observation is in line with recent evidence that laser ablation of centrosome from polarized cells abolished cellular capacity to maintain its cytoskeletal asymmetry and directional migration.[33] Hence, an intact centrosome is indispensable during directional cell migration, which conserves and reorganizes the microtubule network into an asymmetric polarized phenotype. In CNT-treated endothelial cells, we observe that centrosome destruction led to a cellular failure in organizing their microtubules (Figure 4H *vs* 4I) with loss of radial arrangement of microtubules arising from centriolar region, an authentic sign of intact centrosomes (Figure 4B,E,G). Positioning of the nuclear−centrosome (NC) axis is another hallmark of polarity in most migrating cells.[49] Evidently, in our experiment, NC positioning was very well preserved in migrating endothelial cells in clockwise direction without the CNT treatment (immunostained pericentrin in red and nucleus in blue; Figure 4H), which is conspicuously lost because of OS and CNT toxicity (compare Figure 4H,I). Furthermore, a decrease in cell motility is confirmed with the observed changes in the morphology of focal adhesions. The dynamic assembly and disassembly of focal adhesions at the cell front, center, and rear is a fundamental process of migrating cells.[37,50] The CNT-treated endothelial cells have larger FACs, and relatively large spreading area. This indicates that cells respond to CNT exposure with mature focal adhesions expression in CNT-treated cells, mitigating cell motion and affecting cell chirality formed on micropatterns.[51] Taken together, our data suggest that the lack of mutual coordination and compatibility between microtubules and centrosome in the migration process might constitute the main event in the loss of endothelial cell chirality.[49,52] Studies are underway to explore signaling molecules related to the loss of centrosome integrity and formation of mature focal adhesion complexes.[53] These future directions will certainly complement the findings presented here and will explain in depth the origin of nonchiral behavior in endothelial cells due to CNT toxicity.

Finally, in this study the cells were cultured statically on patterned surfaces. This may not reflect the typical dynamic environment experienced by endothelial cells. Such dynamic fluid shear might alter the interaction between CNTs and endothelial cells as well as cellular responses to CNT exposure. However, our system is based on soft lithography, and it could be easily integrated with microfluidics in the future to study the chiral behavior of endothelial cells under dynamic fluid shear.

CONCLUSION

We have described a novel finding, that SWCNTs cause loss of cell chirality. We observed impaired polarity and orientation in NC axis, preceded by intra- and extracellular oxidative stress. The present discovery puts forth a cascade of novel events arising from carbon nanotube-mediated oxidative stress and

toxicity, which alter important biochemical and physiological events in centrosome integrity and cell polarity, which leads to impaired microtubule assembly, reduced cell migration, and the formation of large FACs. The OS guided homeostatic alteration ultimately results in a loss in preferred directional alignment on micropatterned boundaries.

Our study, then, extends the scope and necessity of studying safety in applications of nanomaterials in biomedicine with a new toxicity paradigm: cell chirality. The model presented in this report could be utilized as an *in vitro* model for rapid evaluation of the influence of nanomaterial toxicity on multicellular chirality and subcellular organ polarity.

METHODS

Carbon Nanotube Preparation. SWCNTs were purchased from Cheap Tubes, Inc. 100 mg of the as-received CNTs (diameter 2−5 nm) (Cheap Tubes) were first"cut" and oxidized by sonicating in piranha (sulphuric and nitric acids in 3:1) for 3 h. 4% metals are present in the as supplied CNTs, and the piranha washing can extract a part of metal. However, a complete removal of metal catalyst has never been reported. After acid reflux, the suspension was washed with Milli-Q water several times by filtering through a 0.8 mm polycarbonate membrane (Millipore). Nanotubes were lyophilized and stored as a dry powder, which was resolubilized in cell culture media with 2-min sonication.[54] Nanotubes were imaged and analyzed with a transmission electron microscope (TEM).

Microcontact Printing. Cell patterning was performed as described in our previous study.[27] First a mold is obtained from SU-8 2050 photoresist (Micro-Chem Corp.) using ultraviolet light and a chromium mask with desired geometric features. Polydimethylsiloxane (PDMS) prepolymer and curing agent (Dow Corning) in 10:1 ratio was poured onto the mold and cured at 70 °C for 4 h. Octadecanethiol (Sigma) was transferred as self-assembly monolayers (SAMs) onto the gold-coated (150 Å in thickness) glass slide with the PDMS stamp (Figure S1, Supporting Information). The slide was then immersed in ethylene glycol-terminated SAM (HS-$(CH_2)_{11}$-EG3, Prochimia) for 3 h. Finally, patterned surfaces were sterilized with ethanol and incubated with 10 μg/mL fibronectin (Sigma) for 30 min before cell seeding.

Cell Culture and CNT Incubation for Dose- and Time-Dependent Study. Endothelial cells at passage 3−5 were maintained in tissue flasks with Endothelial Basal Medium-2 (EBM-2) supplemented with EGM-2 SingleQuot Kit supplement and growth factors (Lonza). C2C12 cells were cultured in DMEM with 10% fetal bovine serum, 1% P/S, 1 mM sodium pyruvate. A stock solution of 1 mg/mL of CNTs was made in the Endothelial Growth Medium (EGM) or in DMEM. CNTs were added at different concentrations (0.5, 1, 5, 10, 50, and 100 μg/mL) in 6 well plates for different days *in vitro* (DIV) (day 1, 3, 5, 7, and 14). Three independent experiments in triplicate were performed. For long-term cultures, media supplemented with CNTs was changed after every 2−3 days. After the time points specified above, cells were washed with PBS, trypsinized, and seeded onto protein-coated patterned surfaces. Once the cells attached, extra cells were washed off with fresh medium. Phase contrast images were taken after overnight incubation at 37 °C and 5% CO_2 when cells reached confluence on the ring pattern.

Cell Viability, Intra- and Extracellular Oxidative Stress Measurements. Viability and proliferation were determined using a colorimetric 3-(4,5-dimethylthiazol-2-yl)-2,5-diphenyltetrazolium bromide (MTT) assay, as per manufacturer instruction. The hUVECs were seeded in 96-well tissue culture plates at a density of 4×10^3 cells per well and incubated overnight prior to the addition of CNTs in EGM of different concentrations, and incubated for another 24 h. Cells without CNTs were used as a control. After, 20 μL of MTT (Sigma) was added and incubated for another 3 h at rt, and the absorbance at 570 nm was recorded on a microplate spectrophotometer (Synergy HT Multi-Mode Microplate Reader, Biotek).

Intracellular OS was assessed *via* mitochondrial staining and measuring the intracellular GSH level (reduced form), a direct indicator of ROS mediated oxidative stress.[55] The cells treated with CNTs in EGM at different concentrations (0.5−100 μg/mL) for 24 h. Cells were washed with PBS, and 1% perchloric acid was added to lyse cell pellets for 10 min on ice. Cell lysate was then centrifuged (15 000 rpm at 4 °C, 5 min) to remove precipitated protein. The supernatant was buffered in KH_2PO_4/EDTA, and *o*-phthaldialdehyde (Sigma) were added and incubated for 30 min at rt. Fluorescence was measured as GSH content using a multiwell plate reader (excitation/emission: 350/420 nm).[56] The GSH readings were normalized by the total protein content measured with the BCA protein assay (Pierce, Rockfold, IL, USA), and have a unit of nM of glutathione per mg of total protein. The reported GSH levels of experimental groups were percentages relative to that of the control.

Hydrogen peroxide production in culture media was measured by Amplex Red hydrogen peroxide detection kit according to the manufacturer's protocol. hUVECs were exposed to CNT at nontoxic, subtoxic, and toxic concentrations. After 24 h incubation, Kreb's Ringers solution was added incubated for another 8 h. The incubated supernatant was further incubated with the Amplex Red horseradish peroxidase reagent solution for 8 h at 37 °C. Fluorescence intensity was measured using Synergy HT Multi-Mode Microplate Reader (Biotek) @excitation/emission 530/590 nm. ROS inhibition studies of hydroxyl and superoxide anions in culture media was carried by incubating cells with CNTs in EGM with 20 mM Mannitol overnight and then micropatterned for LR alignment analysis. Other ROS scavenger, catalase (50 U/mL), and diphenyleneiodonium chloride (DPI) at 1 μM concentration were incubated with hUVECs in presence and absence of CNTs for 24 h. Afterward chiral analysis was performed as explained in above sections.

Immunofluorescence Staining. The multicellular ring patterns were fixed with 4% formaldehyde in cytoskeletal buffer (10 mM MES, 138 mM KCl, 3 mM $MgCl_2$, 2 mM EGTA, and 0.32 M sucrose) for 30 min. For cytoskeleton (actin/tubulin) double staining, the cells were incubated with phalloidin-TRITC (1:400; Invitrogen) and anti-Tubulin-FITC (1:200; Sigma) for 1 h. For the centrosome positioning and focal complex staining on patterned rings, the cells were incubated in 50 μg/mL anti-mouse pericentrin and antivinculin (Abcam) respectively for 1 h. After secondary antibodies staining, samples were fixed in VECTASHIELD mounting media with DAPI (Vector lab).

For mitochondrial staining, Mitro Tracker Deep Red FM (Life Technologies) was used at a working concentration of 100 nM. The cell permeable probe Mitotracker is membrane-potential-dependent dye, which permanently links to thiol groups in mitochondria in both live and fixed cells.

Image analyses including fluorescence quantification and nuclear counting were performed with the NIH ImageJ software.[57]

Cell Chiral Alignment Analysis. A Zeiss-Axiovision microscope was used to capture high-resolution phase contrast images at a resolution of approximately 0.645 μm/pixel. The images were analyzed using a custom-written code in MatLab (MathWorks), which detects intensity gradient and circular statistics in automation. The algorithm determines intensity gradients pixel by pixel with a Gaussian differential filter. An accumulator scheme further determines dominant local direction after dividing an image into subregions, in which the orientation of each pixel follows a von Mises distribution, a circular analogue of the linear normal distribution. Finally, an angle bias map is generated on the basis of the orientation in each subregion and its deviation from the circumferential direction (Figure S2C,

Supporting Information). The standard deviation of LR asymmetry and mean angle were calculated for all subregions, using circular statistics.[58]

Cell Migration and Morphology Analysis. hUVECs in culture (with and without CNTs) were seeded at a low density on gold-coated glass slides. After cells attached, unbound cells were washed, and the dish was transferred into an incubation chamber (37 °C and 5% CO_2), and time-lapse videos were recorded every 5 min at a resolution of 1.56 μm/pixel for a total time of 8−10 h. Sparsely distributed cells were tracked with ImageJ Manual tracking plugin, which allows for quantifying temporal movements of objects between frames in a time-lapse video. A nondestructive grid of crosses was designed, and the plugin retrieves distance traveled by objects between two successive frames. After each run, the plugin generates the distance covered between two frames and intensity of the selected pixel or volume in tabular form between XY and XYZ coordinates as well as velocity.

Cell morphology was quantified and categorized as fibroblastoid or epitheloid, on the basis of cell aspect ratio. The longest vertical (*a*) and horizontal (*b*) distance between the leading and trailing edge of the cell, passing through the nucleus defines CAR, and was calculated as *a*/*b* ratio (Figure S4B, Supporting Information). Quantification was based on phase contrast images captured from live cells. Fibroblastoid cells were defined as those having *a*/*b* ratio greater than 1.5, while epitheloid cells for those having a ratio less than or equal to 1.5.[33]

Statistical Analysis. Clockwise or counterclockwise alignment was determined from calculated biased angles in local regions using MATLAB with the one sample *t* test in linear statistics for the mean angle. The rank test was performed to validate overall biased behavior of the cells considering the number of rings exhibiting either clockwise or counter clockwise alignment. The significance level was set to 0.05 for all statistical analyses. Data was represented by the mean value with the standard error of the mean (SEM) as per commonly used protocols. For ROS inhibition, concentration- and time-dependent studies statistical analysis was conducted using a paired *t* test or an unpaired, two-tailed Student's *t* test.

Conflict of Interest: The authors declare no competing financial interest.

Acknowledgment. L.Q.W. is thankful for the support from National Science Foundation and American Heart Association.

Supporting Information Available: Supplementary figures and tables. This material is available free of charge *via* the Internet at http://pubs.acs.org.

REFERENCES AND NOTES

1. Roco, M. C., Williams, S., Alivisatos, P. *Nanotechnology Research Directions: IWGN Workshop Report*; Kluwer: Dordrecht, The Netherlands, 2000.
2. Peer, D.; Karp, J. M.; Hong, S.; Farokhzad, O. C.; Margalit, R.; Langer, R. Nanocarriers as an Emerging Platform for Cancer Therapy. *Nat. Nanotechnol.* **2007**, *2*, 751–760.
3. Ferrari, M. Cancer Nanotechnology: Opportunities and Challenges. *Nat. Rev. Cancer* **2005**, *5*, 161–171.
4. De La Zerda, A.; Zavaleta, C.; Keren, S.; Vaithilingam, S.; Bodapati, S.; Liu, Z.; Levi, J.; Smith, B. R.; Ma, T.-J.; Oralkan, O.; *et al.* Carbon Nanotubes as Photoacoustic Molecular Imaging Agents in Living Mice. *Nat. Nanotechnol.* **2008**, *3*, 557–562.
5. Shi, X.; von dem Bussche, A.; Hurt, R. H.; Kane, A. B.; Gao, H. Cell Entry of One-Dimensional Nanomaterials Occurs by Tip Recognition and Rotation. *Nat. Nanotechnol.* **2011**, *6*, 714–719.
6. Dvir, T.; Timko, B. P.; Kohane, D. S.; Langer, R. Nanotechnological Strategies for Engineering Complex Tissues. *Nat. Nanotechnol.* **2010**, *6*, 13–22.
7. Duan, X.; Li, Y.; Rajan, N. K.; Routenberg, D. A.; Modis, Y.; Reed, M. A. Quantification of the Affinities and Kinetics of Protein Interactions Using Silicon Nanowire Biosensors. *Nat. Nanotechnol.* **2012**, *7*, 401–407.
8. Joshi, A.; Punyani, S.; Bale, S. S.; Yang, H.; Borca-Tasciuc, T.; Kane, R. S. Nanotube-Assisted Protein Deactivation. *Nat. Nanotechnol.* **2008**, *3*, 41–45.
9. Singhal, R.; Orynbayeva, Z.; Kalyana Sundaram, R. V.; Niu, J. J.; Bhattacharyya, S.; Vitol, E. A.; Schrlau, M. G.; Papazoglou, E. S.; Friedman, G.; Gogotsi, Y. Multifunctional Carbon-Nanotube Cellular Endoscopes. *Nat. Nanotechnol.* **2010**, *6*, 57–64.
10. Welsher, K.; Liu, Z.; Sherlock, S. P.; Robinson, J. T.; Chen, Z.; Daranciang, D.; Dai, H. A Route to Brightly Fluorescent Carbon Nanotubes for Near-Infrared Imaging in Mice. *Nat. Nanotechnol.* **2009**, *4*, 773–780.
11. Kostarelos, K.; Lacerda, L.; Pastorin, G.; Wu, W.; Wieckowski, S.; Luangsivilay, J.; Godefroy, S.; Pantarotto, D.; Briand, J.-P.; Muller, S.; *et al.* Cellular Uptake of Functionalized Carbon Nanotubes is Independent of Functional Group and Cell Type. *Nat. Nanotechnol.* **2007**, *2*, 108–113.
12. Nagai, H.; Okazaki, Y.; Chew, S. H.; Misawa, N.; Yamashita, Y.; Akatsuka, S.; Ishihara, T.; Yamashita, K.; Yoshikawa, Y.; Yasui, H.; *et al.* Diameter and Rigidity of Multiwalled Carbon Nanotubes are Critical Factors in Mesothelial Injury and Carcinogenesis. *Proc. Natl. Acad. Sci. U. S. A.* **2011**, *108*, 1330–1338.
13. Nel, A.; Xia, T.; Madler, L.; Li, N. Toxic Potential of Materials at the Nanolevel. *Science* **2006**, *311*, 622–627.
14. Palomaki, J.; Valimaki, E.; Sund, J.; Vippola, M.; Clausen, P. A.; Jensen, K. A.; Savolainen, K.; Matikainen, S.; Alenius, H. Long, Needle-like Carbon Nanotubes and Asbestos Activate the NLRP3 Inflammasome through a Similar Mechanism. *ACS Nano* **2011**, *5*, 6861–6870.
15. Labrousse, A. M.; Meunier, E.; Record, J.; Labernadie, A.; Beduer, A.; Vieu, C.; Ben Safta, T.; Maridonneau-Parini, I. Frustrated Phagocytosis on Micro-patterned Immune Complexes to Characterize Lysosome Movements in Live Macrophages. *Front. Immunol.* **2011**, *12*, 1–9.
16. Kostarelos, K.; Bianco, A.; Prato, M. Promises, Facts and Challenges for Carbon Nanotubes in Imaging and Therapeutics. *Nat. Nanotechnol.* **2009**, *4*, 627–633.
17. Cheng, W.-W.; Lin, Z.-Q.; Ceng, Q.; Wei, B.-F.; Fan, X.-J.; Zhang, H.-S.; Zhang, W.; Yang, H.-L.; Liu, H.-L.; Yan, J.; *et al.* Single-Wall Carbon Nanotubes Induce Oxidative Stress in Rat Aortic Endothelial Cells. *Toxicol. Mech. Methods* **2012**, *22*, 268–276.
18. Pichardo, S.; Gutiarrez-Praena, D.; Puerto, M.; Sanchez, E.; Grilo, A.; Camean, A. M.; Jos, A. Oxidative Stress Responses to Carboxylic Acid Functionalized Single Wall Carbon Nanotubes on the Human Intestinal Cell Line Caco-2. *Toxicol. In Vitro* **2012**, *26*, 672–677.
19. Lam, C. W.; James, J.; McCluskey, R.; Arepalli, S.; Hunter, R. A Review of Carbon Nanotube Toxicity and Assessment of Potential Occupational and Environmental Health Risks. *Crit. Rev. Toxicol.* **2006**, *36*, 189–217.
20. Manna, S. K.; Sarkar, S.; Barr, J.; Wise, K.; Barrera, E. V.; Jejelowo, O.; Rice-Ficht, A. C.; Ramesh, G. T. Single-Walled Carbon Nanotube Induces Oxidative Stress and Activates Nuclear Transcription Factor-κB in Human Keratinocytes. *Nano Lett.* **2005**, *5*, 1676–1684.
21. Pacurari, M.; Yin, X. J.; Zhao, J.; Ding, M.; Leonard, S. S.; Schwegler-Berry, D.; Ducatman, B. S.; Sbarra, D.; Hoover, M. D.; Castranova, V. Raw Single-Wall Carbon Nanotubes Induce Oxidative Stress and Activate MAPKs, AP-1, NF-κB, and Akt in Normal and Malignant Human Mesothelial Cells. *Environ. Health Perspect.* **2008**, *116*, 1211–1217.
22. Patel, H.; Kwon, S. Multi-Walled Carbon Nanotube-Induced Inflammatory Response and Oxidative Stress in a Dynamic Cell Growth Environment. *J. Biol. Eng.* **2012**, *6*, 1–9.
23. Reddy, A. R. N.; Reddy, Y. N.; Krishna, D. R.; Himabindu, V. Multi Wall Carbon Nanotubes Induce Oxidative Stress and Cytotoxicity in Human Embryonic Kidney (HEK293) Cells. *Toxicology* **2010**, *272*, 11–16.
24. Tay, C. Y.; Gu, H.; Leong, W. S.; Yu, H.; Li, H. Q.; Heng, B. C.; Tantang, H.; Loo, S. C. J.; Li, L. J.; Tan, L. P. Cellular Behavior of Human Mesenchymal Stem Cells Cultured on Single-Walled Carbon Nanotube Film. *Carbon* **2010**, *48*, 1095–1104.

25. Yehia, H. N.; Draper, R. K.; Mikoryak, C.; Walker, E. K.; Bajaj, P.; Musselman, I. H.; Daigrepont, M. C.; Dieckmann, G. R.; Pantano, P. Single-Walled Carbon Nanotube Interactions with HeLa Cells. *J. Nanobiotechnol.* **2007**, *5*, 1–8.
26. Nel, A. E.; Madler, L.; Velegol, D.; Xia, T.; Hoek, E. M. V.; Somasundaran, P.; Klaessig, F.; Castranova, V.; Thompson, M. Understanding Biophysicochemical Interactions at the Nano-Bio Interface. *Nat. Mater.* **2009**, *8*, 543–557.
27. Wan, L. Q.; Ronaldson, K.; Park, M.; Taylor, G.; Zhang, Y.; Gimble, J. M.; Vunjak-Novakovic, G. Micropatterned Mammalian Cells Exhibit Phenotype-Specific Left-Right Asymmetry. *Proc. Natl. Acad. Sci. U. S. A.* **2011**, *108*, 12295–12300.
28. Wan, L. Q.; Vunjak-Novakovic, G. Micropatterning Chiral Morphogenesis. *Commun. Integr. Biol.* **2011**, *4*, 745–748.
29. Wan, L. Q.; Ronaldson, K.; Guirguis, M.; Vunjak-Novakovic, G. Micropatterning of Cells Reveals Chiral Morphogenesis. *Stem Cell Res. Ther.* **2013**, *4*, 24–30.
30. Chen, C. S.; Mrksich, M.; Huang, S.; Whitesides, G. M.; Ingber, D. E. Geometric Control of Cell Life and Death. *Science* **1997**, *276*, 1425–1428.
31. Zhang, Y.; Xu, Y.; Li, Z.; Chen, T.; Lantz, S. M.; Howard, P. C.; Paule, M. G.; Slikker, W.; Watanabe, F.; Mustafa, T.; *et al.* Mechanistic Toxicity Evaluation of Uncoated and PEGylated Single-Walled Carbon Nanotubes in Neuronal PC12 Cells. *ACS Nano* **2011**, *5*, 7020–7033.
32. Wu, S.; Zhou, F.; Zhang, Z.; Xing, D. Mitochondrial Oxidative Stress Causes Mitochondrial Fragmentation *via* Differential Modulation of Mitochondrial Fission−Fusion Proteins. *FEBS J.* **2011**, *278*, 941–954.
33. Nicole, M. W.; Elliot, L. B.; Justin, L.; Michael, W. B. An Intact Centrosome Is Required for the Maintenance of Polarization During Directional Cell Migration. *PLoS One* **2010**, *5*, e15462–e15473.
34. Bornens, M. Organelle Positioning and Cell Polarity. *Nat. Rev. Mol. Cell Biol.* **2008**, *9*, 874–886.
35. Luders, J.; Stearns, T. Microtubule-Organizing Centres: A Re-Evaluation. *Nat. Rev. Mol. Cell Biol.* **2007**, *8*, 161–167.
36. Nigg, E. A.; Stearns, T. The Centrosome Cycle: Centriole Biogenesis, Duplication and Inherent Asymmetries. *Nat. Cell Biol.* **2011**, *13*, 1154–1160.
37. Geiger, B.; Spatz, J. P.; Bershadsky, A. D. Environmental Sensing Through Focal Adhesions. *Nat. Rev. Mol. Cell Biol.* **2009**, *10*, 21–33.
38. Balaban, N. Q.; Schwarz, U. S.; Riveline, D.; Goichberg, P.; Tzur, G.; Sabanay, I.; Mahalu, D.; Safran, S.; Bershadsky, A.; Addadi, L.; *et al.* Force and Focal Adhesion Assembly: A Close Relationship Studied Using Elastic Micropatterned Substrates. *Nat. Cell Biol.* **2001**, *3*, 466–472.
39. Heister, E.; Brunner, E. W.; Dieckmann, G. R.; Jurewicz, I.; Dalton, A. B. Are Carbon Nanotubes a Natural Solution? Applications in Biology and Medicine. *ACS Appl. Mater. Interfaces* **2013**, *5*, 1870–1891.
40. Liu, D.; Yi, C.; Zhang, D.; Zhang, J.; Yang, M. Inhibition of Proliferation and Differentiation of Mesenchymal Stem Cells by Carboxylated Carbon Nanotubes. *ACS Nano* **2010**, *4*, 2185–2195.
41. Singh, A. V.; Khare, M.; Gade, W. N.; Zamboni, P. Theranostic Implications of Nanotechnology in Multiple Sclerosis: A Future Perspective. *Autoimmune Dis.* **2012**, *2012*, 160830–160841.
42. Li, R, Bowerman, B. *Symmetry Breaking in Biology*, 2nd ed.; Cold Spring Harbor Laboratory Press: Cold Spring Harbor, NY, 2010; p 3475.
43. Xavier, S.-P.; Vito, C.; Romaric, V.; Ester, A.; Dhananjay, T. T.; Elsa, B.; James, P. B.; Jeffrey, J. F.; Xavier, T. Mechanical Waves During Tissue Expansion. *Nat. Phys.* **2012**, *8*, 628–634.
44. Zhang, D.; Yi, C.; Qi, S.; Yao, X.; Yang, M. Effects of Carbon Nanotubes on the Proliferation and Differentiation of Primary Osteoblasts. *Methods Mol. Biol.* **2010**, *625*, 41–53.
45. Jones, C. F.; Grainger, D. W. *In Vitro* Assessments of Nanomaterial Toxicity. *Adv. Drug Delivery Rev.* **2009**, *61*, 438–456.
46. Lin, S.; Zhao, Y.; Nel, A. E.; Lin, S. Zebrafish: An *In Vivo* Model for Nano EHS Studies. *Small* **2013**, *9*, 1608–1618.
47. Morimoto, Y.; Horie, M.; Kobayashi, N.; Shinohara, N.; Shimada, M. Inhalation Toxicity Assessment of Carbon-Based Nanoparticles. *Acc. Chem. Res.* **2013**, *46*, 770–781.
48. Uttara, B.; Singh, A. V.; Zamboni, P.; Mahajan, R. T. Oxidative Stress and Neurodegenerative Diseases: A Review of Upstream and Downstream Antioxidant Therapeutic Options. *Curr. Neuropharmacol.* **2009**, *7*, 65–74.
49. Luxton, G. W. G.; Gundersen, G. G. Orientation and Function of the Nuclear-Centrosomal Axis During Cell Migration. *Curr. Opin. Cell Biol.* **2011**, *23*, 579–588.
50. Fraley, S. I.; Feng, Y.; Krishnamurthy, R.; Kim, D.-H.; Celedon, A.; Longmore, G. D.; Wirtz, D. A Distinctive Role for Focal Adhesion Proteins in Three-Dimensional Cell Motility. *Nat. Cell Biol.* **2010**, *12*, 598–604.
51. Wolfenson, H.; Bershadsky, A.; Henis, Y. I.; Geiger, B. Actomyosin-Generated Tension Controls the Molecular Kinetics of Focal Adhesions. *J. Cell Sci.* **2011**, *124*, 1425–1432.
52. Mogilner, A.; Keren, K. The Shape of Motile Cells. *Curr. Biol.* **2009**, *19*, 762–771.
53. Broussard, J. A.; Webb, D. J.; Kaverina, I. Asymmetric Focal Adhesion Disassembly in Motile Cells. *Curr. Opin. Cell Biol.* **2008**, *20*, 85–90.
54. Dinu, C. Z.; Zhu, G.; Bale, S. S.; Anand, G.; Reeder, P. J.; Sanford, K.; Whited, G.; Kane, R. S.; Dordick, J. S. Enzyme-Based Nanoscale Composites for Use as Active Decontamination Surfaces. *Adv. Funct. Mater.* **2010**, *20*, 392–398.
55. Singh, A.; Oldani, A.; Cartelli, D.; Parazzoli, D.; Gemmati, D.; Orioli, E.; Montani, E.; Zeri, G.; Zamboni, P.; Vyas, V. Investigation of *In Vitro* Cytotoxicity of the Redox State of Ionic Iron in Neuroblastoma Cells. *J. Neurosci. Rural Pract.* **2012**, *3*, 301–310.
56. Hissin, P. J.; Hilf, R. A Fluorometric Method for Determination of Oxidized and Reduced Glutathione in Tissues. *Anal. Biochem.* **1976**, *74*, 214–226.
57. Collins, T. ImageJ for Microscopy. *Biotechniques* **2007**, *43*, 25–30.
58. Fish, N. *Statistical Analysis of Circular Data*; Cambridge University Press: Cambridge, U.K., 1993.